H1prelim-08-132 Submitted to

34th International Conference on High Energy Physics, ICHEP08, 30th July - 5th August, 2008, Philedelphia

Abstract: **867**

Parallel Session **QCD/Lattice**

Electronic Access: www-h1.desy.de/h1/www/publications/conf/conf_list.html

Measurement of $\mathrm{K}^{*\pm}$ Production in Deep Inelastic ep Scattering at HERA

H1 Collaboration

Abstract

A first measurement of $K^*(892)^\pm$ vector mesons, observed through the decay chain $K^*(892)^\pm \to K_s^0\pi^\pm$, in neutral current deep-inelastic ep scattering with the H1 detector are presented. The analysis is based on data taken in the HERA-II running period. Inclusive cross sections are presented as a function of the various kinematic variables. The phase space of the events is restricted to $5 < Q^2 < 100$ GeV^2, $0.1 < y_{e\Sigma} < 0.6$, $-1.5 < \eta_{(K^*)} < 1.5$ and $p_{T(K^*)} > 1$ GeV. The results are compared to predictions of leading order Monte Carlo models matched with the parton showers.

1 Introduction

The measurement of the inclusive particle production cross section gives direct information to understand the hadronization process and to test the fragmentation models. Higher vector meson resonances and their dynamics are closely related to the original partons, while vector mesons are copiously produced and thus better suited to a study of hadronization process.

Light vector meson measurements give direct information about the suppression factor for the strange quark pair production. The study of $K^*(892)^\pm$ has been made by different experiments but with high statistical and systematic uncertainties. With a large number of hadronic events as collected by the H1 experiment an accurate analysis can be performed. The large data sample is particularly important for the understanding of the mass spectrum.

The production of strange quark and its subsequent hadronization in *ep* collisions constitutes an important benchmark test for QCD based models, and for the applicability of perturbative QCD to hard process.

The analysis presented in this paper compares the Monte Carlo (MC) modeled prediction of the final state particle composition with *ep* collision data. One parameter of particular interest is the strangeness suppression factor λ_s. Heavy ion collision data [1] consistently gives lower strange suppression than the e^+e^- annihilation processes [2]. In the *ep* collisions the suppression is different in the photon fragmentation region from that in the proton fragmentation region. Strange quarks are mainly produced in pairs from the vacuum, so the observations above suggests that vacuum properties are not process independent as the suppression is not universal. The latter is assumed in all MC models. A difference in cross section between K^{*+} and K^{*-} might tell something about the possible asymmetric quark sea in the proton.

2 Experimental Set-up

2.1 H1 Detector

The analysis performed with the data taken with the H1 detector from 2005 to 2007, when HERA[1] collided electrons or positrons[2] with energy of $E_e = 27.5\,\text{GeV}$ with protons of $E_p = 920\,\text{GeV}$, yielding a center-of-mass energy of 318 GeV. The results are based on the sum of the e^-p and e^+p samples, corresponding to integrated luminosities of 166.90 pb^{-1} and 134.99 pb^{-1}, respectively.

A detailed description of the H1 detector can be found elsewhere [3]. A brief outline of the components that are the most relevant for this analysis is given here. A right-handed Cartesian coordinate system is used to describe the orientation of the detector, such that the z-axis follows the direction of the proton beam. The polar angle θ is measured with respect to this axis and the pseudorapidity η is given by η = - ln tan $(\frac{\theta}{2})$. The origin of the coordinate system is the nominal interaction point within the detector.

[1]**H**adron **E**lektron **R**ing **A**nlage

[2]Hereafter, both e^+ and e^- are referred to as electrons, unless explicitly stated otherwise.

Charged particles are tracked in the central tracking detector (CTD), which covers the region $15^\circ < \theta < 165^\circ$. The principal components of CTD are the central jet chambers, CJC1 and CJC2 [4]. These are complemented with a central silicon vertex detector (CST) [5]. CJC1 and CJC2 consist of 56 wires parallel to the z-axis and placed in a homogeneous magnetic field 1.16 T. The main purpose of the CJC1 and CJC2 is to provide an accurate measurement in the $r - \phi$ plane, hence their sense wires run parallel to the beam-pipe. The transverse momentum resolution for full-length tracks is $\sigma(p_T)/p_T \simeq 0.005 p_T \oplus 0.0015$ [6].

The tracking detectors are surrounded by a Liquid Argon Calorimeter (LAr) [7] in the forward region which has a polar angle coverage of $4^\circ < \theta < 154^\circ$ and full azimuthal acceptance. In the backward region $153^\circ < \theta < 178^\circ$, particle energies are measured by a lead-scintillating fiber spaghetti calorimeter (SpaCal) [8] with an electromagnetic and hadronic sections. These calorimeters provide energy and angular reconstruction for final state particles from the hadronic system. For high Q2 LAr is used for the electron. Deep Inelastic Scattering (DIS) at low Q^2 events are identified by the energy deposits of the scattered electron in the SpaCal calorimeter.

The luminosity is determined from the rate of Bethe-Heitler process $ep \rightarrow ep\gamma$, measured using a photon detector located close to the beam pipe at z = -103 m, in the backward direction.

2.2 Event selection

Events are triggered by an electromagnetic energy cluster in the SpaCal calorimeter. The kinematic variables the four momentum transfer squared Q^2 of the exchanged virtual photon and in-elasticity $y_{e\Sigma}$ are determined using the electron-sigma method [9].

DIS offline event selection is based on the following requirements:

- $E_e^{'} > 11\,\mathrm{GeV}$, where $E_e^{'}$ is the scattered electron energy in the SpaCal calorimeter. This cut ensures a well reconstructed electron and suppresses the background from photo-production events in which the scattered electron escapes undetected in the rear beam-pipe.
- $5 < Q^2 < 100~\mathrm{GeV}^2$, the four momentum transfer squared Q^2 of the exchanged virtual photon.
- $35 < \Sigma_i(E_i - p_{z,i}) < 70$ GeV. In order to suppress the photo-production background the sum of the differences between the total energy E_i and the longitudinal momentum $p_{z,i}$ of all final state particles is restricted.
- $0.1 < y_{e\Sigma} < 0.6$, where $y_{e\Sigma}$ is in-elasticity calculated with the electron-sigma method.
- The z-position of the event vertex, z_{vtx}, determined from CTD tracks, is required to be within the range $-35 < z_{vtx} < 35$ cm nominal vertex position. In order to correctly determine the vertex position at least two well reconstructed central tracks are required. This cut removes the background events from non-*ep* interactions.

2.3 Reconstruction of K$^{*\pm}$ Candidates

The principal stage in the $K^{*\pm} \rightarrow K^0_s\pi^\pm$ selection process is the identification of neutral kaons K^0_s mesons. The search for the K^0_s is performed via the decay $K^0_s \rightarrow \pi^+\pi^-$ which has the branching ratio of 0.6920 ± 0.0005. Two oppositely charged central tracks in the CTD which originate from a secondary vertex were considered as K^0_s decay products. The conditions which each track had to fulfill are given in the following. Each track is required to have a minimum transverse momentum p_T with respect to the beam direction $p_T > 120$ MeV and pseudo-rapidity $-1.5 < \eta < 1.5$ to ensure that the track is well contained within the acceptance of the CTD.

The angle in the *xy* plane between the vector linking the primary and secondary vertices and the charged track direction in the rest frame of the K^0_s candidate, θ^*,is required to be as $|cos(\theta^*)| < 0.95$. K^0_s candidates should have a radial decay length above than 2 cm.

Furthermore, to reject the photon conversion background both tracks are assigned electron masses and considered to come from photo conversion if the invariant mass of the pair is less than 50 MeV. The contamination from $\Lambda \rightarrow p\pi^-$ and $\bar{\Lambda} \rightarrow \bar{p}\pi^+$ decays is suppressed by requiring that the invariant mass of the track pair, $m_{p\pi}$, within a ± 12 MeV window around the nominal Λ mass. The higher momentum track is assumed to be that of a proton and the lower that of a pion.

The track pairs that originate from a common secondary vertex resulting from the decay of a neutral particle is termed as V^0. The K^0_s or V^0 candidates are classified and identified by a variable called Podolanski-Armenteros parameter

$$p_\perp = \frac{P_+ \cdot P_- \cdot \sin\theta}{P_+ + P_-} \tag{1}$$

where P_+ and P_- are the momenta of the positively and negatively charged tracks in the laboratory frame, respectively. θ is the angle between two momentum vectors of tracks. $p_\perp$ is required $p_\perp > 0.11$ GeV. The transverse momentum p_T of K^0_s candidates should exceed 0.5 GeV.

For further analysis, only K^0_s candidates with a reconstructed mass window of $470 < M_{(\pi^+\pi^-)} < 520$ MeV around the nominal mass of 497.6 MeV were retained. The invariant mass spectrum of K^0_s candidates is shown in Fig. 1. The signal distribution is fitted with the T-student function while the polynomial function is used for fitting the background distribution. The number of K^0_s mesons which yield from the fit is 1319190.

A third charged track which is assumed to be a pion is combined with the K^0_s candidate in order to construct a $K^{*\pm}$ candidate. The third charged track is required to originate from a primary vertex with the same p_T, η, and radiation length cuts as applied for the K^0_s selection.

The nominal value of the K^0_s mass assigned to K^0_s candidates and additional cuts are applied on the combination of K^0_s and $\pi^\pm$, $p_{T(K^0_s\pi^\pm)} > 1$ GeV and $|\eta_{(K^0_s\pi^\pm)}| < 1.5$. Finally, the invariant mass of $K^{*\pm}$ candidates were obtained.

After having applied the selection cuts described above the signal is still governed by large combinatorial background. In order to yield a correct number of $K^{*\pm}$ a proper fit to the invariant mass distribution plays an important role in this analysis.

3 Signal Extraction

The mass distribution of the signal is described with the relativistic Breit-Wigner function

$$BW(m) = \frac{m}{q} \cdot \frac{\Gamma'_K}{(m^2 - m^2{}_K)^2 + (m_K \cdot \Gamma'^2_K)} \quad (2)$$

where m is the mass of K^*, m_K is the central mass of the K^* mass distribution, and Γ'_K is defined as

$$\Gamma'_K(m) = \Gamma_K \cdot (\frac{q(m)}{q(m_K)})^{2l+1} \cdot \frac{m_K}{m} \quad (3)$$

where Γ_K is the natural width of the $K^{*\pm}$, q is the momentum transfer to each decay particle in the center of mass system and l is the relative angular momentum of the decay products. Since the $K^{*\pm}$ are vector mesons decaying into two pseudo-scalar mesons, $l = 1$. The natural width Γ_K of $K^{*\pm}$ is fixed to its PDG value of 50.8 MeV. The mass position m_K is the free parameter of the fit function.

According to the generators strategy, in the MC simulation the K^* signal is described by a so-called non-relativistic Breit-Wigner function:

$$BW(m) = \frac{\Gamma_K}{(m_0 - m)^2 + \frac{\Gamma_K^2}{4}} \quad (4)$$

The background function parametrization is chosen as

$$BG(m) = P_1 \cdot (m_0 - (m_{K^0} + m_\pi)^{P_2}) \cdot exp(P_3 m + P_4 m^2 + P_5 m^3) \quad (5)$$

Here, P_1, P_2, P_3, P_4 and P_5 are free parameters. The background function is used for both data and MC. Invariant mass spectra of $K_s^0 \pi^\pm$ combinatons is shown in Fig. 2. The number of $K^{*\pm}$ mesons which yield from the fit is 78819.

4 Monte Carlo Simulation

Monte Carlo (MC) simulations are used in this analysis for the determination of the detector acceptance and the extraction of the signal. The acceptance correction is determined from events generated with RAPGAP 3.1 [10] and DJANGOh 1.4 event generators.

RAPGAP 3.1 generates events with DGLAP parton showers matched to leading order O(α_s) matrix elements. The direct and resolved photon processes are generated separately and latter added. MRST2004 [11] is used for the parton density parameterizations.

The event generator DJANGOh simulates the deep inelastic lepton-proton scattering including both QCD and QED radiative effects and allows for the event generation according to QCD cascade models or matrix elements. The matrix elements describe the effects from perturbative QCD to first order in α_s due to boson gluon fusion and virtual gluon emission. QCD cascades are generated using the color dipole model as implemented in ARIADNE. The Lund string fragmentation as implemented in the event simulation program JETSET is used to obtain the complete hadronic final state. At low hadronic masses, SOPHIA is used instead of LEPTO.

The color dipole model (CDM) approach is represented by the ARIADNE [16] MC program. The CTEQ6L [17] proton parton distribution functions are used for DJANGOh.

In all MC models, the fragmentation of the final state partons has been performed using the LUND [13] string model as implemented in JETSET [14] . In this model, the strange quark suppression is described by a parameter $\lambda_s = P(s)/P(q)$. Here, $P(s)$ is the probability of the strange production from vacuum during the fragmentation process. $P(q)$ is the probability of the light quarks (u, d) production from vacuum during the fragmentation process. The value of parameter $\lambda_s = 0.286$ was determined by the ALEPH collaboration [15] and is here used for both the generators.

All events generated with RAPGAP 3.1 and DJANGOh 1.4 are passed through a full GEANT [18] simulation of the H1 detector and through the same reconstruction and analysis program as used for the data.

5 Systematic Uncertainties

The various systematic uncertainties are considered. The total systematic error per bin is obtained by adding all different systematic errors in quadrature. The dominant errors are listed below.

- The systematic uncertainty of the luminosity measurement is 3.62%.
- The scattered electron energy $E_e^{'}$ has been varied by $\pm 1\%$. The resulting systematics has been found to be 3.4% [19].
- The uncertainty on the measurement of the polar angle of the scattered electron θ_e leads to a systematic error of 2% [19].
- The uncertainty of the description of the trigger correction leads to a systematic error of 2%.
- The resulting systematic error due to the uncertainty of track efficiency is 2% per track [20].
- The uncertainty attributed to the model dependence is derived by comparing acceptance corrections obtained with RAPGAP 3.1 and DJANGOH 1.4, leading to a systematic error overall 3%, changing bin to bin up to 9%.

- A systematic uncertainty on the background distribution is performed by using the different functions such as 3rd order polynomial and Chebyshev polynomials. The resulting uncertainty is from 2.6% upto 7.8%.
- Besides the errors due to the fit function and the model dependency, the determination of the position of the primary vertex is one of the sources of systematic uncertainty of 2.5% per K^* [20].
- The systematic error of the reconstruction of the number of K^* has been found as 1%.
- Photo-production background has been estimated as 0.3% [20].
- Due to the limited statistics of MC events, the systematic error is determined as 2.2%.
- The sailor and seagull decay topologies of K_s^0 leads to a 3% systematic uncertainty.

6 Results

Differential cross sections for the $K^{*\pm}$ production are measured for $5 < Q^2 < 100\,\mathrm{GeV}^2$, $0.1 < y_{e\Sigma} < 0.6$, $p_{T(K*)} > 1\,\mathrm{GeV}$, $|\eta_{(K*)}| < 1.5$ and presented as a function of transverse momentum p_T, pseudo-rapidity η, four momentum squared of virtual photon Q^2, Feynman-x x_F, the transverse momentum squared P_T^{*2} and the center-of-mass energy of the hadronic final state W. The radiative corrections are not applied to the calculated cross-sections. The comparison between the measured inclusive differential cross sectionsto the LO MC (DJANGOh1.4 and RAPGAP3.1) are shown in the figures 3, 4, 5, 6, 7 and 8. P_T, η and Q^2 were measured in the laboratory frame while x_F, P_T^{*2} and W in hadronic center of mass system. The contributions from the various quark flavors on the proton side are shown in figures 9, 10, 11, 12, 13 and 14. The total measured inclusive cross-section is

$$\sigma(ep \to eK^*X) = 7.36 \pm 0.087(stat) \pm 0.88(sys.)nb. \tag{6}$$

7 Conclusions

$K^*(892)^\pm$ vector mesons, observed through the decay chain $K^*(892)^\pm \to K_s^0\pi^\pm$, in neutral current deep-inelastic ep scattering have been measured first time at HERA. The inclusive production cross-sections as functions of the event kinematics and final state variables were presented in the phase space of $5 < Q^2 < 100, 0.1 < y_{e\Sigma} < 0.6$ GeV^2, $p_{T(K*)} > 1\,\mathrm{GeV}$, and $|\eta_{(K*)}| < 1.5$. The measurement has been compared to the predictions of leading order Monte Carlo models matched with the parton showers. DJANGOh describes the data better than RAPGAP. In the production of K* the u and d quark contributions are the prominent in overall distributions. It is hard to disentangle the strange content of the proton as the measurement is dominated by fragmentation.

References

[1] C. Adler *et al.*, STAR Collaboration, $K^*(892)^0$ Production in Relativistic heavy ion collisions at $\sqrt{s_{NN}} = 130\,\mathrm{GeV}$, Phys. Rev. **C66**, (2002).
J. Adams *et al.*, STAR Collaboration, $K^*(892)$ Resonance Production in $Au + Au$ and $p + p$ collisions at $\sqrt{s_{NN}} = 200\,\mathrm{GeV}$ at STAR, Phys. Rev. **C71**, (2005).

[2] G. Abbidendi *et al.*, OPAL Collaboration, Eur. Phys. **C17**, 373 (2000).

[3] I. Abt *et al.*, H1 Collaboration, The H1 Detector at HERA, Nucl. Instr. Meth., **A386**. p.310-347, (1997).
I. Abt *et al.*, H1 Collaboration, The Tracking Calorimeter and Muon Detectors of H1 Experiment at HERA, Nucl. Instr. Meth., **A386**. p.348-396, (1997).

[4] J. Burger *et al.*, The Central Jet Chamber of the H1 Experiment, Nucl. Instrum. Meth., **A279** p.217, (1989).

[5] D. Pitzl *et al.*, Nucl. Instrum. Meth., **A454** p.334, (2000).

[6] C. Kleinwort, Contribution to LHC Tracking and Alignment Workshop, CERN, 2006.

[7] B. Andrieu *et al.*, Nucl. Instrum. Meth., **A336** p.460 (1993).

[8] T. Nicholls et al., Performance of an Electromagnetic Lead/Scintillating Fiber Calorimeter for the H1 Detector, Nucl. Instrum. Meth. **A374**, p.149-156 (1996).
D. Reyna, Modifications to SPACAL for H1 High Luminosity Operation and the Effect on Acceptance, H1-Internal Note H1-11/98-555, DESY (1998).

[9] U. Bassler, G. Bernardi, On the Kinematic Reconstruction of Deep Inelastic Scattering at HERA: The Sigma Method, DESY-94-231, Nucl. Instrum. Meth. **A361**, p.197 (1995), [hep-ex/9412004].

[10] H. Jung, Hard Diffractive Scattering in High Energy ep Collisions and the Monte Carlo Generator RAPGAP, Comp. Phys. Commun., **86** p.147, (1995).

[11] A. D. Martin, R. G. Roberts, W. J. Stirling and R. S. Thorne, Phys. Lett. B 604 (2004) [arXiv:hep-ph/0410230].

[12] G. A. Schuller and H. Spiesberger, in *Proc. of the Workshop on HERA Physics*, edited by W. Buchmuller and G. Ingelman, DESY, Hamburg, **vol. 3** p.1419, (1992).

[13] T. Sjöstrand, The Lund Monte Carlo For Jet Fragmentation and e^+e^- Physics: Jetset version 6.2, Comp. Phys. Commun., **39** p.347, (1986).

[14] T. Sjöstrand, High Energy Physics Event Generation with PYTHIA 5.7 and JETSET 7.4, Comp. Phys. Commun., **82** p.74, (1994).

[15] R. Barate *et al.*, Studies of Quantum Chromodynamics with the ALEPH Detector, Phys. Rept., **294** (1998) 1.

[16] L. Lönnblad, Ariadne Version 4: A Program for Simulation of QCD Cascades Implementing the Colour Dipole Model, Comp. Phys. Commun., **71** (1992) 15.

[17] J. Pumplin, D. R. Stump, J. Huston, H. L. Lai, P. Nadolsky and W.K. Tung, JHEP 0207, **012**, (2002) [arXiv:hep-ex/9910045].

[18] R. Brun *et al.*, GEANT3, Technical Report, CERN-DD/EE/84-1, CERN, (1987).

[19] H1 Collaboration, Strangeness Production at Low Q2 in Deep Inelastic ep Scattering at HERA, submitted to XVI International Workshop on Deep-Inelastic Scattering, DIS 2008, London.

[20] H1 Collaboration, Dstar production at low Q2 with the H1 detector, submitted to 34th International Conference on High Energy Physics, ICHEP 2008, Philedelphia, Abstract-855.

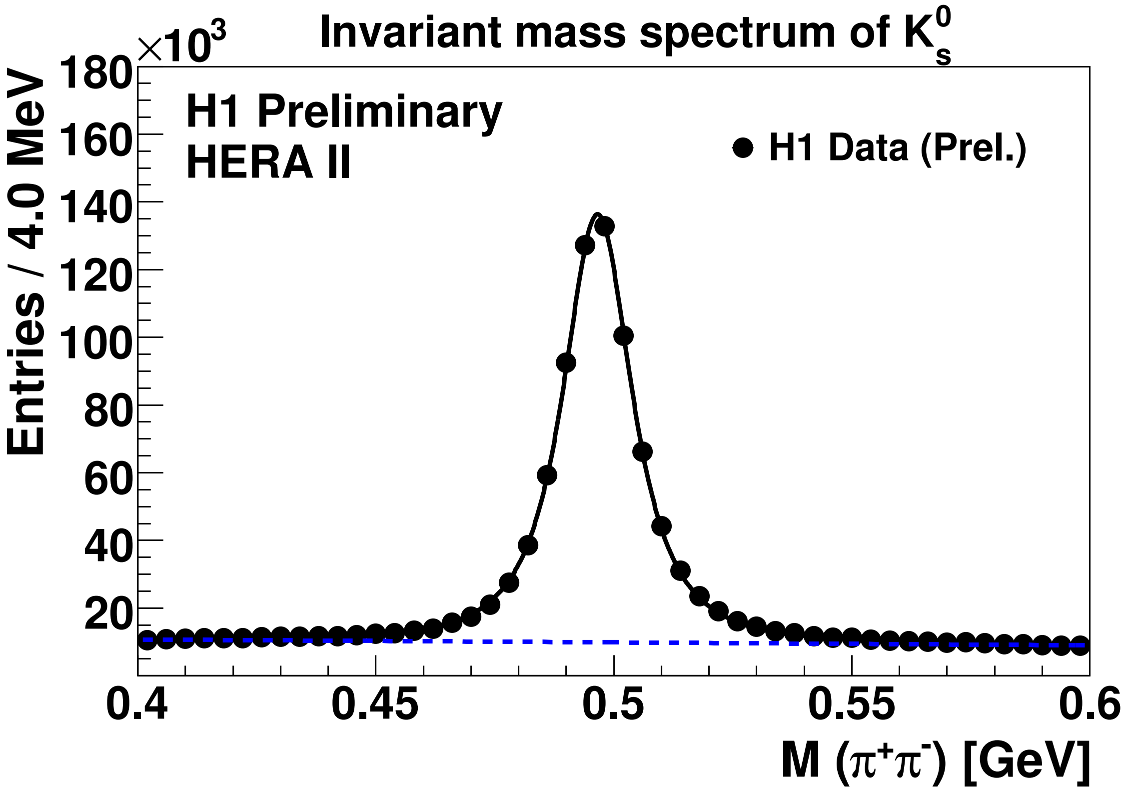

Figure 1: Invariant mass spectrum of the $K_s^0 \to \pi^+\pi^-$ candidates. The points correspond to the observed data events. The distribution is fitted with a t-student function and a polynomial background function. The background is represented with the dashed line.

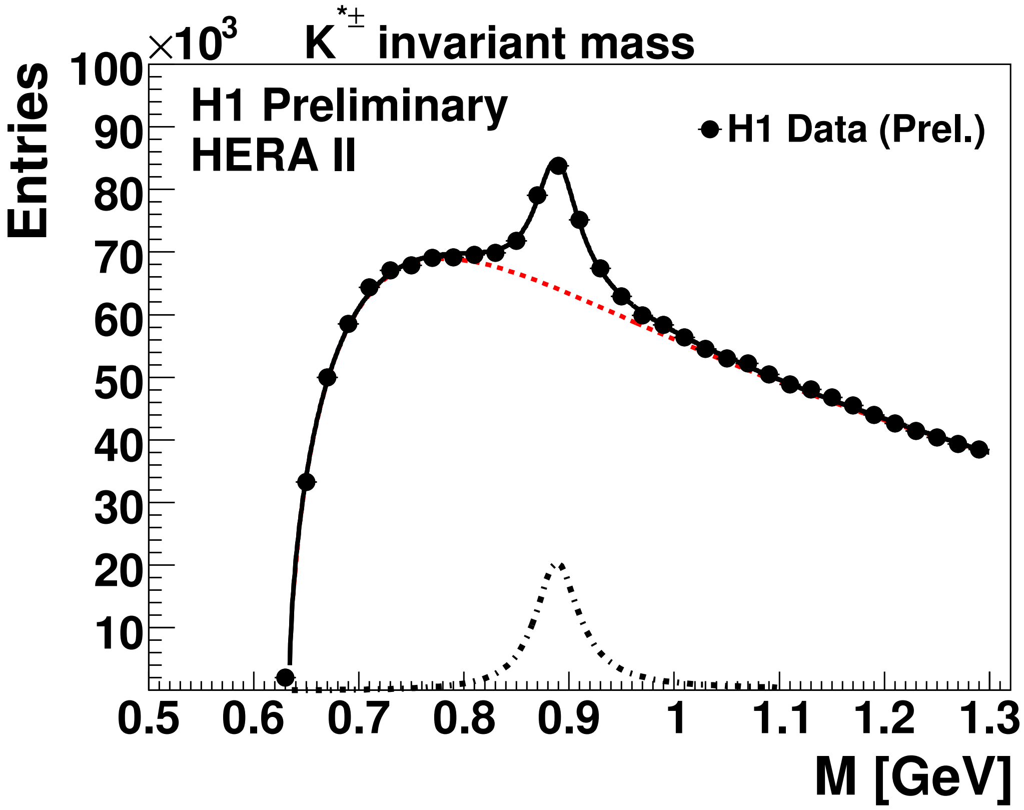

Figure 2: Invariant mass spectra of $K_s^0\pi^\pm$ combinations after application of the cuts mentioned in details in the text. The distribution is fitted with a relativistic Breit-Wigner function (solid line) and a background function (dashed line). The signal is shown with dash-dotted lines.

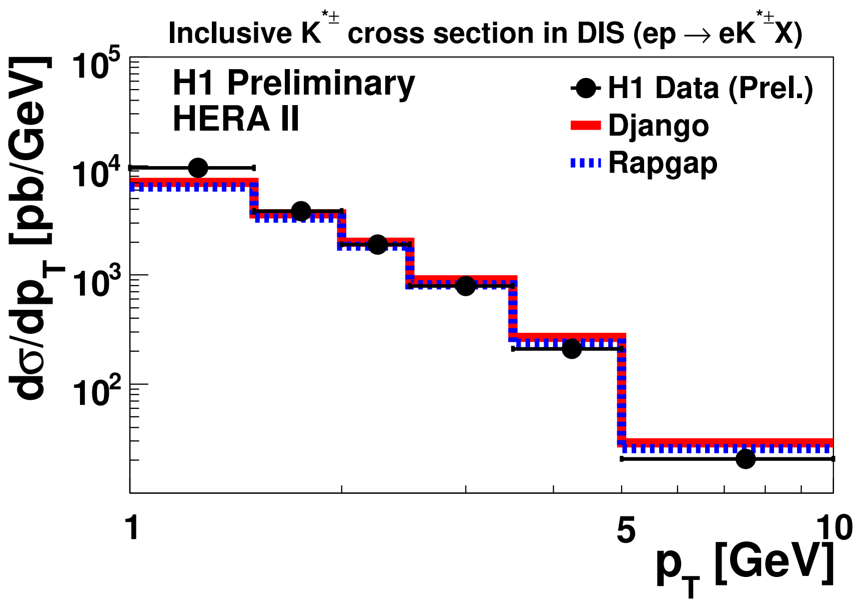

Figure 3: The measured inclusive differential cross section as a function of the transverse momentum p_T. The cross sections is measured in visible range defined by $p_{T(K*)} > 1\,\mathrm{GeV}$, $|\eta_{(K*)}| < 1.5$, $5 < Q^2 < 100\ \mathrm{GeV}^2$ and $0.1 < y_{e\Sigma} < 0.6$. The inner error in the figure represents the statistical error, while the outer is the statistical and the systematic errors added in quadrature. The measured cross section is compared to the DJANGOH1.4 (continuous red) and RAPGAP3.1 (dashed blue) calculations.

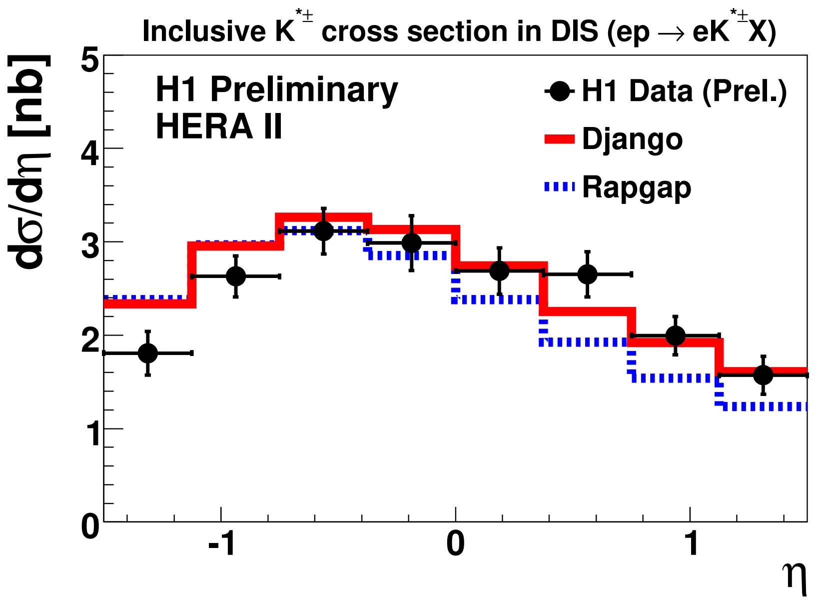

Figure 4: The measured inclusive differential cross section as a function of the pseudo-rapidity η. For details see Fig. 3.

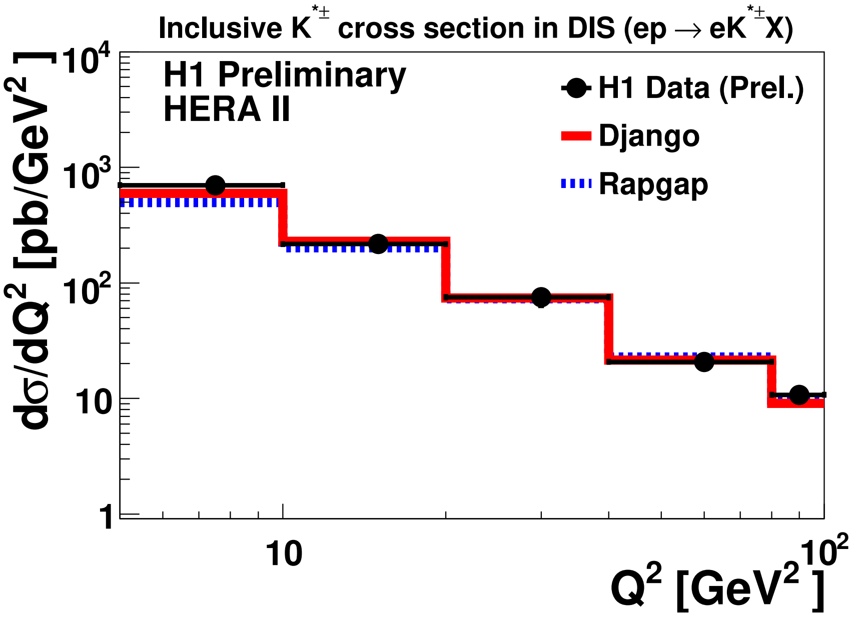

Figure 5: The measured inclusive differential cross section as a function of the four momentum squared Q^2. For details see Fig. 3.

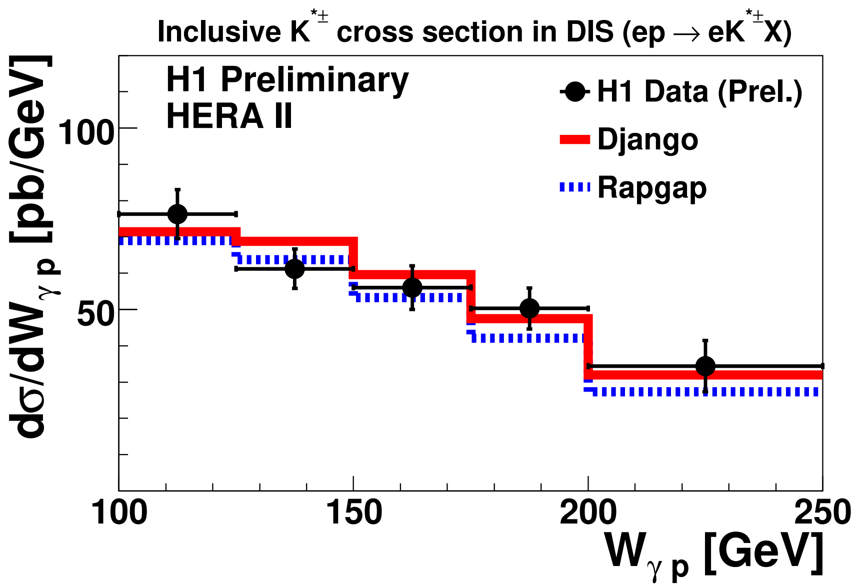

Figure 6: The measured inclusive differential cross section as a function of the centre-of-mass energy of the hadronic final state $W_{\gamma p}$. For details see Fig. 3.

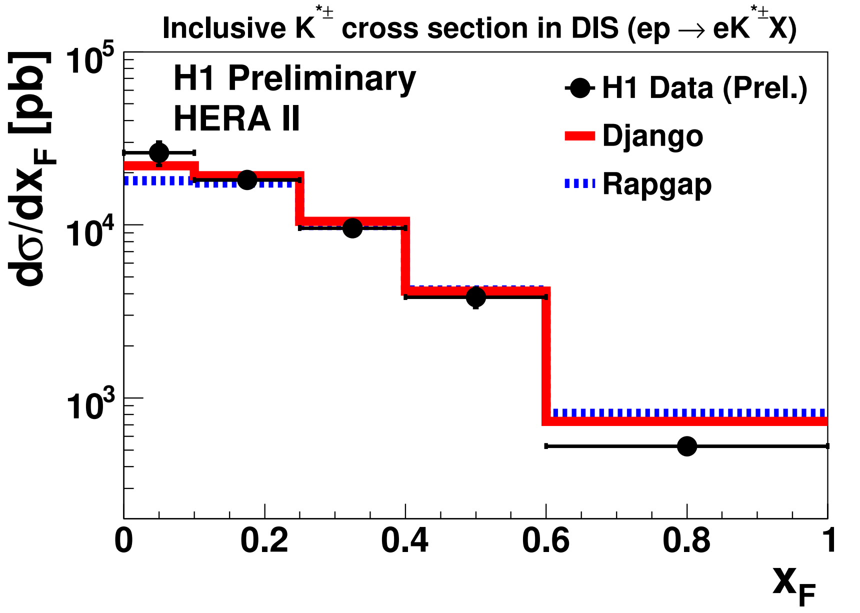

Figure 7: The measured inclusive differential cross section as a function of the Feynman-x x_F. For details see Fig. 3.

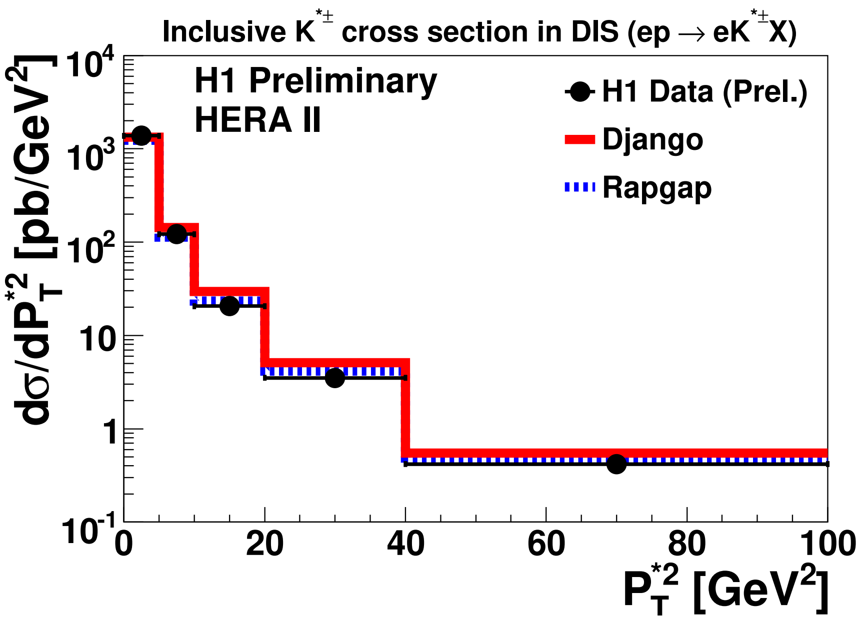

Figure 8: The measured inclusive differential cross section as a function of the transverse momentum squared in the hadronic final state P_T^{*2}. For details see Fig. 3.

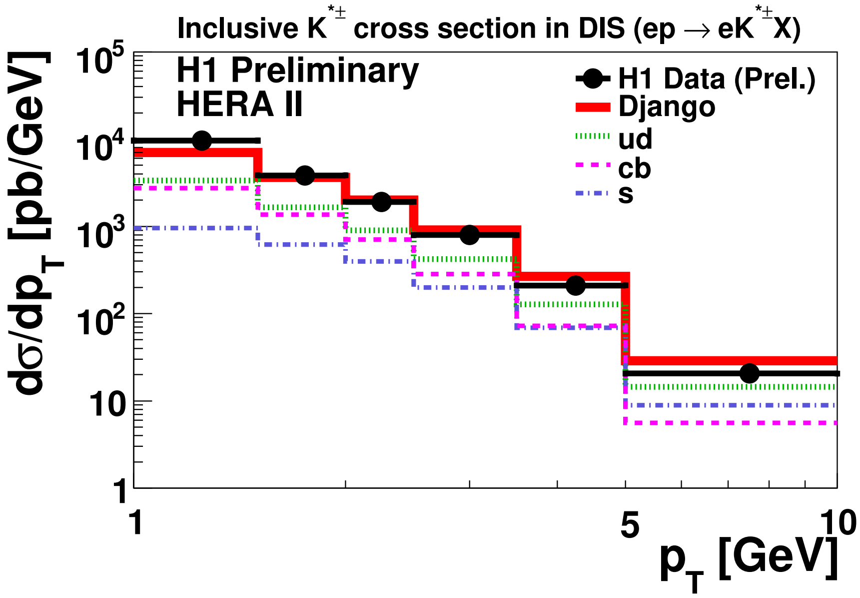

Figure 9: The measured inclusive differential cross sections as a function of the transverse momentum p_T. The cross sections are measured in visible range defined by $p_{T(K*)} > 1\,\mathrm{GeV}$, $|\eta_{(K*)}| < 1.5$, $5 < Q^2 < 100$ GeV^2 and $0.1 < y_{e\Sigma} < 0.6$. The inner error in the figure represents the statistical error, while the outer is the statistical and the systematic errors added in quadrature. The quark contributions (ud (green dotted lines), cb (magenta dashed lines), and s (blue dash-dotted lines)) are shown.

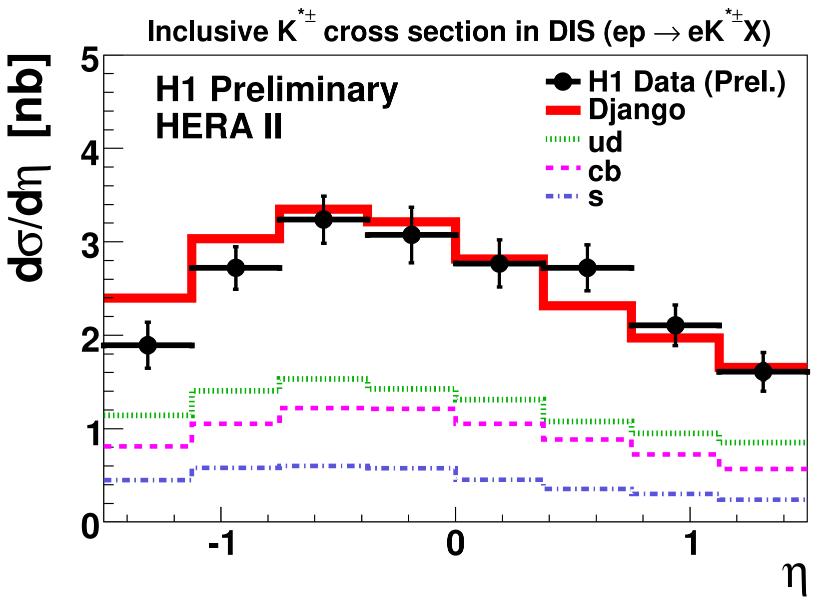

Figure 10: The measured inclusive differential cross sections as a function of the pseudo-rapidity η. For details see Fig. 9.

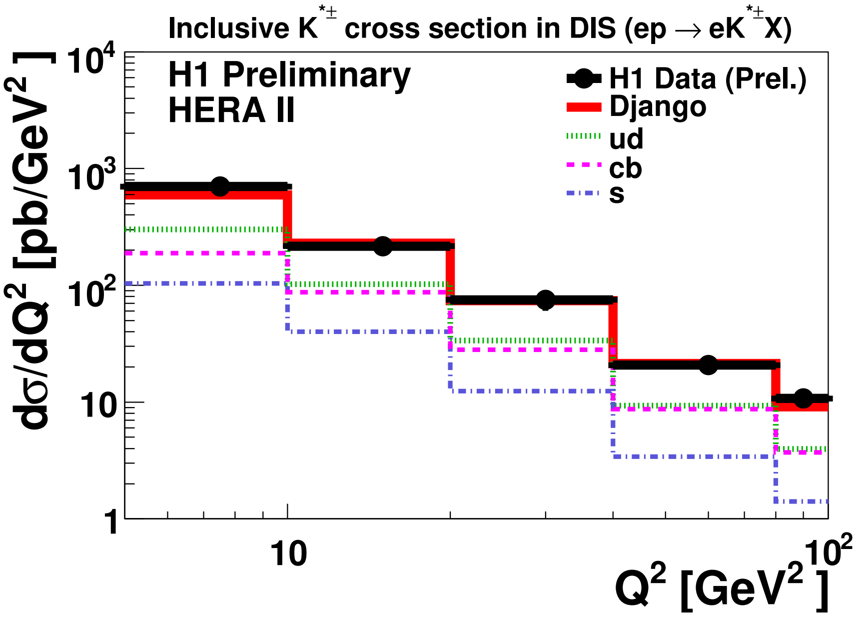

Figure 11: The measured inclusive differential cross sections as a function of the four momentum squared Q^2. For detatils see Fig. 9.

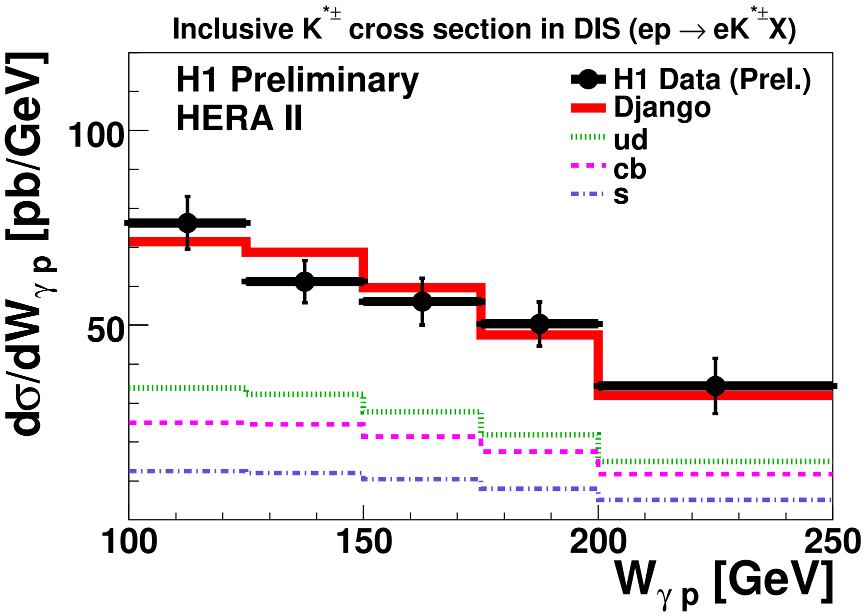

Figure 12: The measured inclusive differential cross sections as a function of the centre-of-mass energy of the hadronic final state W. For detatils see Fig. 9.

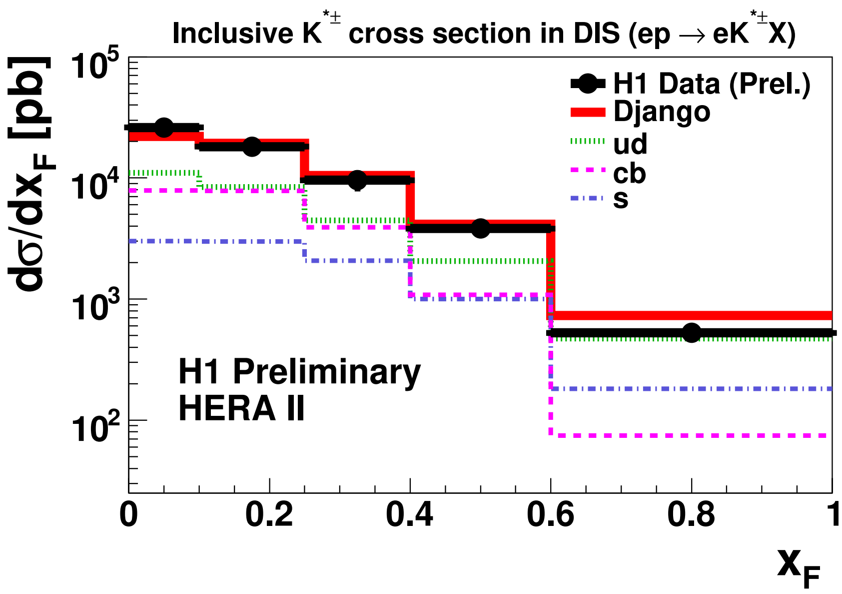

Figure 13: The measured inclusive differential cross sections as a function of the Feynman-x x_F. For detatils see Fig. 9.

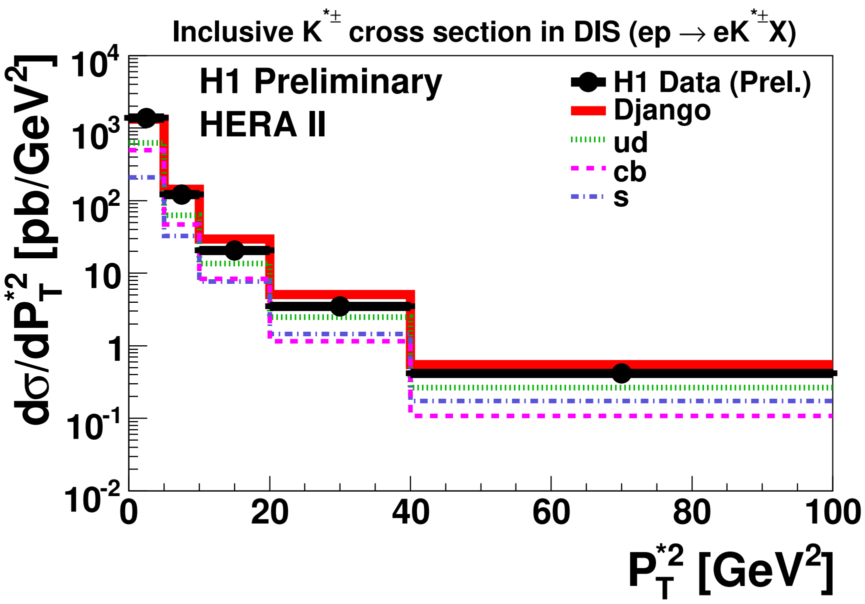

Figure 14: The measured inclusive differential cross sections as a function of the transverse momentum squared in the hadronic fianl state P_T^{*2}. For detatils see Fig. 9.